Adv. Opt. Techn., Vol. 1 (2012), pp. 187–194 • Copyright © 2012 THOSS Media and De Gruyter. DOI 10.1515/aot-2012-0017

Research Article

Hybrid hyperchromats for chromatic confocal sensor systems

Matthias Hillenbrand[1,*], Beate Mitschunas[1], Christian Wenzel[2], Adrian Grewe[1], Xuan Ma[1], Patrick Feßer[1], Mohamed Bichra[1] and Stefan Sinzinger[1]

[1] Fachgebiet Technische Optik, IMN MacroNano®, Technische Universität Ilmenau, Ilmenau, 98693, Germany
[2] Development Lighting, Hella KGaA Hueck & Co., Lippstadt, 59552, Germany

* Corresponding author
e-mail: matthias.hillenbrand@tu-ilmenau.de
Received April 12, 2012; accepted May 30, 2012

Abstract

The combination of diffractive and refractive elements in hybrid optical systems allows for precise control of the longitudinal chromatic aberration. We provide comprehensive design strategies for hybrid hyperchromatic lenses that maximise the longitudinal chromatic aberrations. These lenses are mainly used in chromatic confocal sensor systems for efficient non-contact profilometry as well as for measurements of distances and wall thicknesses of transparent materials. Our design approach enables the tailoring of the sensor properties to the specific measurement problem and assists designers in finding optimised solutions for industrial applications. We, for example, demonstrate a hybrid system that significantly exceeds the longitudinal chromatic aberration of purely diffractive elements.

Keywords: chromatic confocal sensing; diffractive optics; lens design; micro-optics; optical metrology.

1. Introduction

Owing to dispersion the focal lengths of refractive and diffractive optical elements (DOEs) vary with wavelength. Refractive lenses of different materials as well as diffractive components are commonly combined in achromatic and apochromatic systems with heavily reduced chromatic aberrations [1–3]. They can also be integrated in optical systems with maximised longitudinal chromatic aberration. Such systems are called hyperchromats [4, 5] and are used, for example, in combination with the confocal principle [6–8] for non-contact optical metrology. So far, the main applications are surface profilometry as well as measurements of distances and layer thicknesses of transparent media [4, 5, 9–37]. Measurement ranges vary from a few µm [17, 29] to several mm [22, 37]. Various authors have used DOEs in confocal imaging systems to exploit their high dispersion compared to refractive optical elements [24–37].

We present comprehensive design strategies for chromatic confocal sensor systems. Our approach combines paraxial and collinear theory with the potential of ray-tracing based optimisation. It is suitable for refractive, diffractive as well as hybrid diffractive-refractive optical systems and enables novel solutions with unique properties. Power balancing between the diffractive and refractive components gives precise control over the measurement range. The proposed design strategies can be easily combined with further application-specific system requirements. Thus, they are of great importance for the development of optimised sensor solutions tailored to specific industrial applications. After an introduction to the chromatic confocal principle we present our design strategy as well as two design examples. Specifically, we show that hybrid systems may easily exceed the longitudinal chromatic aberration of purely diffractive elements. The power of our approach is proven by experimental results.

2. Chromatic confocal principle

The working principle of a fibre-based chromatic confocal sensor is shown in Figure 1. Light from a polychromatic, fibre-coupled source is incident upon the hyperchromatic objective lens. Owing to dispersion each wavelength is focussed at a different distance behind the lens. The distance between the foci for the maximum and the minimum wavelengths defines the measurement range. If an object (i.e., a reflecting or scattering surface) is brought within the measurement range, the light is partially reflected back into the objective lens. The wavelength focussed onto the object surface (λ_2 in Figure 1) is also focussed at the fibre exit surface. All other wavelengths (e.g., λ_1 in Figure 1) are subject to defocus and reduced coupling efficiency. The spectral distribution of the light coupled back into the fibre is analysed with a spectrometer. Because all but the focussed wavelengths are damped, the wavelength of maximum power is directly related to the distance between the sensor and the surface to be measured. Thus, the confocal system performs an efficient depth to wavelength coding. For measurements of layer and wall thicknesses the reflections from the front and back surfaces of the object yield two maxima in the spectral distribution. By evaluating the spectral distance between these two maxima the layer or wall thickness can be determined. Three-dimensional (3D) profilometry can, for example, be realised through lateral scanning of the object under test.

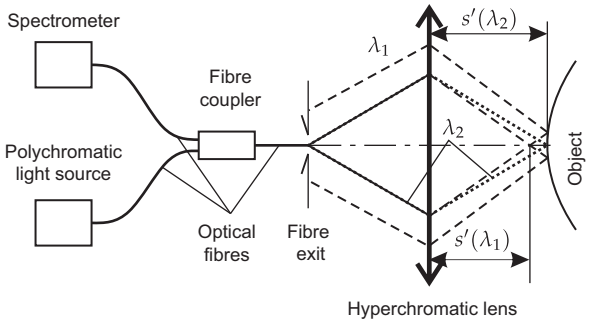

Figure 1 Fibre-based chromatic confocal sensor principle.

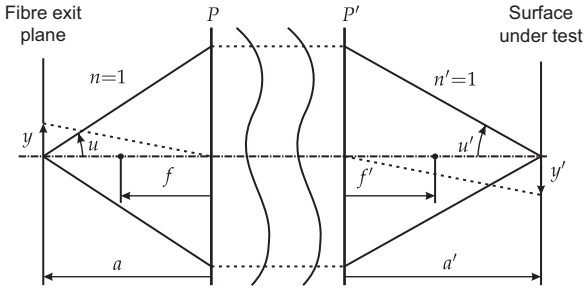

Figure 2 Collinear setup of the hyperchromatic lens with principal planes P and P'.

3. Design strategies for hybrid hyperchromatic lenses

The main design criteria for chromatic confocal sensor systems include:

- the working distance,
- the measurement range,
- axial and lateral resolution,
- the allowed tilt angle of the object under test,
- speed and efficiency, as well as
- size, cost, and stability.

In particular, fibre-based systems are well suited for constricted industrial environments as they allow for easy separation of the light source, the spectrometer, and the electronics from the flexible, small and robust sensor head. In contrast to the classical confocal setup where the pinhole size and the object space numerical aperture (NA) can be defined separately, fibre-based setups are constrained to a limited range of fibres with predefined core diameters and numerical apertures. The object and image space properties of an optical system in air ($n'=n$, $f'=f$) are linked through the sine condition, Newton's equation, and the lateral magnification [38]:

$$y'\sin u'=y\sin u;\ \frac{1}{a'}-\frac{1}{a}=\Phi'=\frac{1}{f'};\ M=\frac{y'}{y}=\frac{a'}{a}. \tag{1}$$

Throughout this paper non-primed symbols are related to object space while primed symbols represent parameters in image space. Figure 2 shows the collinear setup of the hyperchromatic lens. a, u, y (a', u', y') are the object (image) distance, the object (image) space marginal ray angle, and the object (image) height. In air, the object and image space numerical apertures are related to the marginal ray angles by $NA=\sin u$ and $NA'=\sin u'$, respectively. The focal length and focal power of the lens are given by $f'=-f$ and $\Phi=1/f'$, respectively. Thus, for a given fibre, working distance and NA' the basic paraxial properties of the optical system including the focal power can be determined.

Based on the collinear layout the individual lenses of the optical system have to be selected. For this purpose a thin lens model can be used taking into account the dispersive characteristics of the individual lenses. A schematic sketch of a possible system of thin lenses is shown in Figure 3. The measurement range of a chromatic confocal sensor is influenced by the wavelength range of the light source, the paraxial layout, and the dispersion characteristics of the optical components. It is defined as the difference between the working distances for the minimum wavelength λ_1 and the maximum wavelength λ_2 of the source spectrum. Various authors (e.g., [1]) have shown that this distance, which is equivalent to the longitudinal chromatic aberration, can be approximated for a system of thin lenses by the equation:

$$\Delta s'_n=-\frac{s'^2_n}{h^2_n}\sum_{i=1}^{n}\frac{\Phi_i h_i^2}{V_i}. \tag{2}$$

s'_n denotes the distance from the last surface of the system to the image plane, whereas h_i defines the intersection heights of the paraxial marginal ray with the thin lenses. The focal powers of these lenses are given by Φ_i and the parameters s_n, h_i, and Φ_i are evaluated at the reference wavelength λ_0. The total focal power of the system is defined as [1]:

$$\Phi=\frac{1}{h_1}\sum_{i=1}^{n}h_i\Phi_i. \tag{3}$$

The dispersive behaviour of the diffractive and refractive optical elements is defined by the Abbe number V_i [2, 39]:

$$V_i=\begin{cases}\dfrac{n(\lambda_0)-1}{n(\lambda_1)-n(\lambda_2)} & \text{for refractive elements,}\\[2ex] \dfrac{\lambda_0}{\lambda_1-\lambda_2} & \text{for diffractive elements.}\end{cases} \tag{4}$$

For the standard wavelengths $\lambda_0=\lambda_d$, $\lambda_1=\lambda_F$ and $\lambda_2=\lambda_C$, the Abbe numbers of Schott preferred glasses range approximately from 21 to 85 [40]. By contrast, diffractive elements always have an Abbe number of -3.45 for these wavelengths. Thus, they are very well suited for the realisation of an increased measurement range of the confocal system with a minimum number of optical components. Whereas a chromatic confocal setup consisting of a single DOE can be sufficient for some applications, more complex hybrid diffractive-refractive systems are useful in the majority

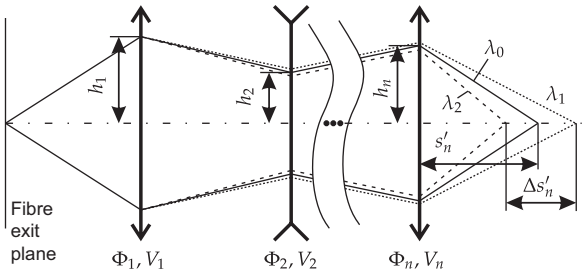

Figure 3 Longitudinal chromatic aberration of a system of thin lenses.

of cases. Even for a given paraxial setup with predefined parameters (magnification, diameter, numerical aperture, working distance) and for a given light source (with fixed values λ_1 and λ_2), a precise control of the measurement range is possible through the focal power distribution between the diffractive and refractive elements. By combining positive diffractive with negative refractive elements (or vice versa), systems can be built that significantly exceed the longitudinal chromatic aberration of a single diffractive element. It is worth noting that the measurement range increases with the squared value of the working distance. Thus, a much larger measurement range can be realised for systems with long working distances.

The axial resolution of chromatic confocal sensor systems depends on several factors. The most important parameters are the spectral resolution of the spectrometer, the signal-to-noise ratio of the sensor system, as well as the numerical aperture and the imaging performance of the objective lens. To evaluate the distance between the sensor and a single reflecting or scattering surface the peak wavelength of the spectral signal has to be determined. For well-corrected objective lenses the accuracy of this evaluation mainly depends on the spectral resolution of the spectrometer and the noise level. Layer and wall thickness measurements additionally require that the maxima of the reflected signals can be separated. In this case the spectral bandwidths of the individual signals have to be small enough. Several authors have discussed the influence of the numerical aperture on the spectral bandwidth of the reflected signal. An extensive summary of publications on this topic is provided by Gu [41] for monochromatic confocal sensor systems. The image space numerical aperture of the sensor is also related to the maximum tolerable slope angle of the object surface under test. According to the law of reflection the light cone reflected at the surface will be tilted by twice the slope angle of the surface. As a result, only a portion of the reflected light passes the aperture of the optical system and contributes to the spectrometer signal. The theoretical limit is reached when the half cone angle equals the slope angle of the surface. Hence, higher numerical apertures also enable higher tilt angles. Finally, it is worth mentioning that the numerical aperture usually changes with wavelength. In this case, it will be higher for the wavelengths focussed closer to the sensor.

Another important issue in the design of hybrid diffractive-refractive optical systems is diffraction efficiency. In scalar diffraction theory the polychromatic diffraction efficiency of multilevel diffractive optical elements at normal incidence is given by [42]:

$$\eta_q(\lambda,P)=\left[\frac{\sin\left(\pi\frac{q}{P}\right)}{\pi\frac{q}{P}}\right]^2\left[\frac{\sin\left(P\left(\frac{1}{2}\phi(\lambda)-\pi\frac{q}{P}\right)\right)}{P\cdot\sin\left(\frac{1}{2}\phi(\lambda)-\pi\frac{q}{P}\right)}\right]^2, \tag{5}$$

with

$$\phi(\lambda)=\frac{2\pi\lambda_0}{\lambda P}\frac{n(\lambda)-1}{n(\lambda_0)-1}. \tag{6}$$

The number of levels is denoted by P while q specifies the diffraction order. The wavelength-dependent diffraction efficiency of 4-level and 8-level fused silica DOEs is visualised in Figure 4. For this simulation we used the simplifying assumption $n(\lambda)=n(\lambda_0)$. As the diffraction efficiency reduces with increasing distance between the working and the design wavelength, a small wavelength band has to be selected to warrant high diffraction efficiency over the full measurement range. Alternatively, efficiency achromatised diffractive optical elements could be used [43]. These special components show nearly constant diffraction efficiency over a long wavelength band, while Eqs. (2) to (4) are still valid.

Whereas an increased longitudinal chromatic aberration is a necessary property of the sensor, monochromatic aberrations should be kept at a minimum for all wavelengths to warrant the desired resolution. The aberration behaviour of systems based on a single on-axis fibre or pinhole is dominated by third and higher order spherical aberrations. As these lead to a lateral spread of the point spread function, a smaller amount of energy is coupled back into the fibre and the focused wavelength is partially attenuated. Thus, the spectral peak recorded by the spectrometer broadens while

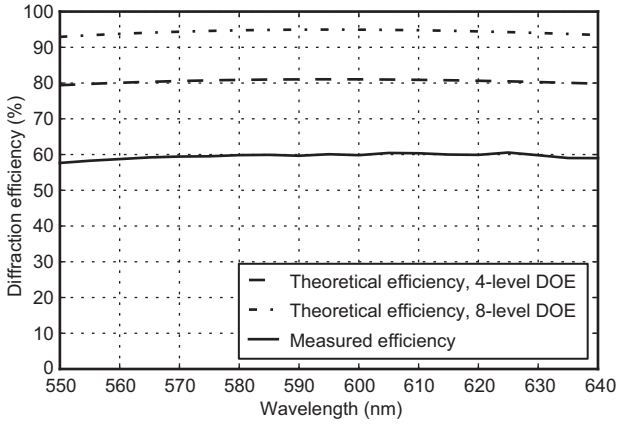

Figure 4 Comparison between the measured diffraction efficiency of DOE 1 and the results from scalar theory.

its maximum intensity decreases. In particular, in systems for wall and layer thickness measurements these effects lead to lower axial resolution. When the surface under test is tilted, the double-pass system loses its axial symmetry and can no longer be accurately described by Seidel aberration theory. A promising approach to the analysis of optical systems without rotational symmetry is given by nodal aberration theory [44]. Typically, a decrease of system performance and axial resolution can be expected for increasing slope angles of the surface under test. We observed this decrease, for example, in numerical simulations and practical experiments with a NA 0.4 chromatic confocal sensor optimised for tilt angles up to 20° [19].

As every optical system has specific aberrations, no universal approach is available. Therefore, balancing between the different orders of spherical aberrations as well as defocus is a valid strategy. This can be efficiently done by numerical, ray-based optimisation with the previously developed paraxial layout as a starting system. DOEs with aspherical phase functions can be realised without additional effort and cost. Thus, it is possible to correct for monochromatic aberrations [33, 35] and to reduce the number of elements in comparison to a purely refractive system of spherical lenses. Although an increased numerical aperture is beneficial with respect to the diffraction limited resolution and the allowed slope of the surface under test, it is usually related to increasing monochromatic aberrations. By contrast, the benefits of an increased numerical aperture are reversed by the negative effects of monochromatic aberrations. At the same time the local period of the DOE decreases with diameter. In paraxial approximation the minimum feature size $\omega_{\min}$ of a P-level DOE is given by [39]:

$$\omega_{\min}=\frac{\lambda_0}{NA_{DOE}\cdot P}, \tag{7}$$

with NA_{DOE} being the numerical aperture of the individual *DOE*. As the minimum feature size is restricted by the available fabrication technology, DOEs can only be realised up to a specific numerical aperture. Thus, there are several conflicting priorities that have to be resolved during the design process. The simultaneous requirements of a high NA and a long working distance will lead to large systems with corresponding costs and weight. To satisfy the minimum feature size and efficiency restrictions, the DOEs will have a relatively low focal power, which is directly related to less longitudinal chromatic aberrations and a smaller measurement range. Thus, the final layout of the sensor will always be application-specific and dependent on the expertise of the lens designer who has to find the optimum solution with respect to these constraints. The development of complex starting systems can be simplified by collinear dimensioning tools (e.g., [45]).

4. Chromatic confocal sensor designs

To demonstrate the potential of our approach, we discuss two design examples. The hybrid system 1 is aimed at maximisation of the longitudinal chromatic aberration. System 2 consists of two diffractive elements and combines a long measurement range with a maximum numerical aperture of 0.20. Both systems are designed to perform as point sensors for distance measurements. For optimum diffraction efficiency over the full measurement range the spectral bandwidth has been restricted to 90 nm. The reference, minimum, and maximum wavelengths are given by λ_0=595 nm, λ_1=550 nm, λ_2=640 nm, respectively. The systems have been designed for use with a multimode gradient-index fibre of 50 µm core diameter and NA of 0.20. Both systems were optimised with commercial ray-tracing software and the layouts including the geometrical dimensions are shown in Figure 5. The DOEs are described using the continuous phase function:

$$\delta=a_1\rho^2+a_2\rho^4+a_3\rho^6, \text{ with } \rho=r/r_{Norm}. \tag{8}$$

The coefficients of the three DOEs are given in Table 1. All three DOEs exhibit a minimum local period of 3.2 µm at the outer rims of the elements. With these restrictions we realised a measurement range of 27.2 mm for system 1, whereas system 2 has a measurement range of 16.8 mm. The comparison between these two values clearly shows that hybrid systems can easily outperform purely diffractive systems with respect to longitudinal chromatic aberration. As mentioned in the design section, the image space numerical aperture of the sensors is wavelength-dependent (see Table 2). Both systems show a nearly diffraction limited performance for

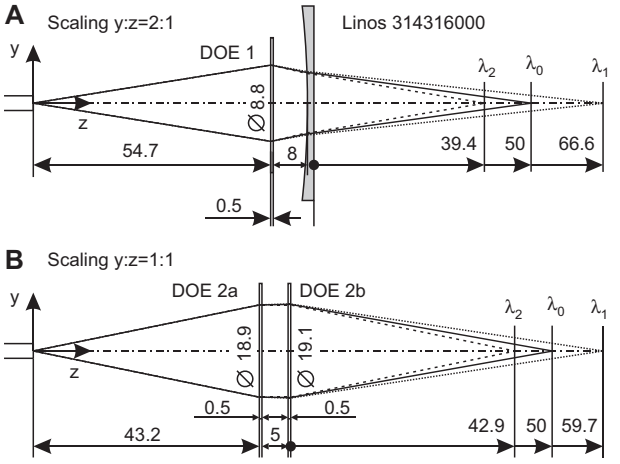

Figure 5 Layout of the two demonstrator systems: (A) hybrid system 1, (B) diffractive system 2. Dimensions are given in mm.

Table 1 Coefficients of the DOEs used in the chromatic confocal system designs.

DOE #	r_{Norm}	a_1	a_2	a_3
1	4.4	-4287.61206	0.46324364	-0.07827469
2a	8.9	-9999.99997	578.9449802	24.30795403
2b	9.1	-8412.17725	-457.704825	-13.6305263

Table 2 Nominal performance of the hyperchromatic lenses.

System	λ (nm)	a' (mm)	Strehl ratio	NA'
1	550	66.6	0.995	0.054
	595	50.0	1.000	0.069
	640	39.4	0.993	0.084
2	550	59.7	0.988	0.147
	595	50.0	0.938	0.173
	640	42.9	0.980	0.198

all wavelengths. To characterise the imaging performance, the nominal Strehl ratios [46] of both sensors at the reference wavelength, as well as at the maximum and minimum wavelengths are given in Table 2.

5. Experimental results

In this section, we present experimental results for system 1. The DOE for the prototype was fabricated in fused silica using contact lithography and inductively coupled plasma reactive ion etching (ICP-RIE). For high diffraction efficiency, a three-step lithographic process with eight resulting phase levels was used in the centre of the DOE. The outer area from 4.4 mm to 8.8 mm diameter was manufactured with four phase levels due to the available minimum feature size of 0.8 µm.

The performance of the system was evaluated with respect to the diffraction efficiency of the DOE, the spectral coding characteristics, and the axial resolution. The polychromatic diffraction efficiency was determined at the full diameter of the DOE using a fibre-coupled monochromator with a xenon arc lamp. The experimental results are compared to the theoretical predictions from scalar diffraction theory in Figure 4. It is important to note that 75% of the DOE area is restricted to four phase levels, whereas only the central part of the DOE was fabricated with eight phase levels. Deviations from the scalar predictions are caused by the limited validity of scalar theory for the feature sizes applied here (compare, e.g., [39])

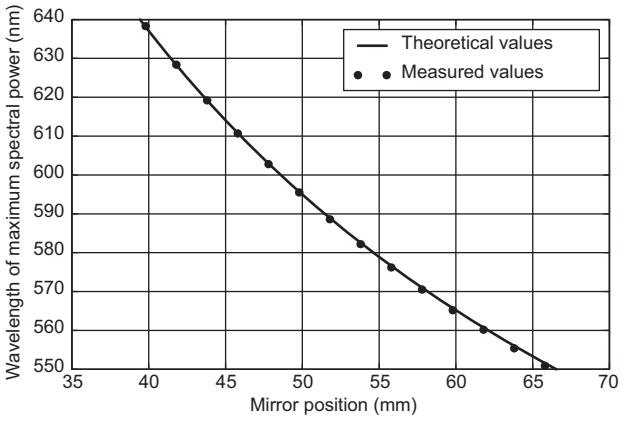

Figure 6 Comparison between the measured and the predicted depth-to-wavelength coding of system 1.

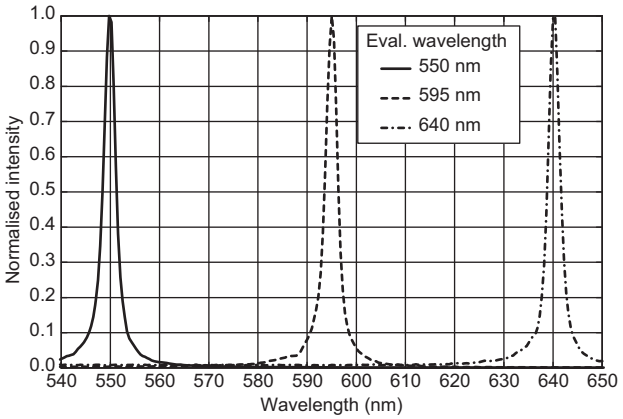

Figure 7 Spectral responses of system 1 at the beginning, the centre, and the end of the measurement range.

as well as by alignment errors during the fabrication of the diffractive element.

The spectral coding characteristics were evaluated by moving a mirror through the measurement range and by recording the wavelengths of maximum intensity at discrete mirror positions. In Figure 6, the resulting depth to wavelength curve is compared to the analytical prediction from the ZEMAX® chromatic focal shift feature. Both curves are in very good agreement and confirm the proposed design strategies.

The spectral bandwidths of the reflected signals were determined by placing a mirror at three positions of the measurement range. The spectral response was recorded with the spectrometer and is shown in Figure 7. Full width at half maximum (FWHM) bandwidths of 2.87 nm, 2.86 nm, and 2.90 nm translate to axial FWHM-depth responses of 0.53 mm, 0.82 mm, and 1.37 mm at the short end, the centre, and the long end of the measurement range, respectively. These values are especially important for layer and wall thickness measurements and could be heavily reduced in a more complex system with higher NA. For distance measurements, the axial resolution of the sensor system is limited by the spectral resolution of our spectrometer. The presented measurements were performed using a Maya2000Pro spectrometer with a spectral resolution of approximately 0.67 nm over the range of 200–1114 nm. This value is related to axial resolutions of 0.13 mm, 0.19 mm, and 0.31 mm at the short end, the centre, and the long end of the measurement range, respectively. These values could be improved with a spectrometer adapted to the 90-nm measurement range.

6. Conclusion

Hyperchromatic lenses employ the inherent dispersion of diffractive and refractive optical components to maximise the longitudinal chromatic aberration. In combination with the confocal sensor principle this colour separation behaviour allows for efficient depth to wavelength coding. The main applications include non-contact profilometry as well as the measurement of distances and wall thicknesses of transparent

materials. Industrial sensors usually demand application-specific designs that fulfil the specific imaging requirements with a system of minimum complexity and cost. In this paper, we presented the first comprehensive treatment of the main design strategies necessary for the efficient development of such tailored chromatic confocal sensor systems. Paraxial and collinear equations were introduced as guidelines for the generation of suitable starting systems. To determine the best shape of the optical components with respect to monochromatic aberration, tolerances, and cost, subsequent optimisation was proposed. The presented strategy is suitable for the development of diffractive, refractive, as well as hybrid diffractive-refractive sensors. Further application-specific requirements (e.g., telecentricity) can be easily integrated into the design process. The proposed techniques were successfully used for the design of two demonstrator systems, which are in excellent agreement with the analytical predictions.

Acknowledgements

This work was funded by the German 'Bundesministerium für Bildung und Forschung' (BMBF) within the projects 'Kompetenzdreieck Optische Mikrosysteme – KD OptiMi' (FKZ: 16SV3700, FKZ: 16SV5473) and 'Optische Mikrosysteme für die hyperspektrale Sensorik (OpMiSen)' (FZK: 16SV5575K), as well as by the Thüringer Ministerium für Bildung, Wissenschaft und Kultur (TMBWK) through the Graduate Research Schools 'Optical Microsystems Technology (OMITEC)' (FZK: PE 104-1-1) and 'Green Photonics' (FZK: B514-10062).

References

[1] R. Kingslake and R. B. Johnson, in 'Lens Design Fundamentals', 2nd ed. (Academic, London, 2010).
[2] T. Stone and N. George, Appl. Optics 27, 2960 (1988).
[3] N. Davidson, A. A. Friesem and E. Hasman, Appl. Optics 32, 4770 (1993).
[4] J. Novak and A. Miks, Optik 116, 165 (2005).
[5] O. Carrasco-Zevallos, R. L. Shelton, C. Olsovsky, M. Saldua, B. E. Applegate, et al., Proc. SPIE 80861D (2011).
[6] M. Minsky, 'Microscopy apparatus', US Patent 3013467.
[7] D. K. Hamilton, T. Wilson and C. J. R. Sheppard, Opt. Lett. 6, 625 (1981).
[8] T. Wilson and C. Sheppard, in 'Theory and Practice of Scanning Optical Microscopy', 2nd ed. (Academic Press, London, 1985).
[9] G. Molesini, G. Pedrini, P. Poggi and F. Quercioli, Opt. Commun. 49, 229 (1984).
[10] O. Akinyemi, A. Boyde, M. A. Browne, M. Hadravsky and M. Petran, Scanning 14, 136 (1992).
[11] M. A. Browne, O. Akinyemi and A. Boyde, Scanning 14, 145 (1992).
[12] M. Maly and A. Boyde, Scanning 16, 187 (1994).
[13] H. J. Tiziani and H. M. Uhde, Appl. Optics 33, 1838 (1994).
[14] H. Perrin, P. Sandoz and G. Tribillon, Pure Appl. Opt. 4, 219 (1995).
[15] H. J. Tiziani, M. Wegner and D. Steudle, Opt. Eng. 39, 32 (2000).
[16] J. McBride and C. Maul, IEICE Trans. Electron. 87, 1261 (2004).
[17] K. Shi, P. Li, S. Yin and Z. Liu, Opt. Express 12, 2096 (2004).
[18] B. S. Chun, K. Kim and D. Gweon, Rev. Sci. Instrum. 80, 073706 (2009).
[19] M. Hillenbrand, B. Mitschunas and S. Sinzinger, Proc. DGaO P1 (2009).
[20] S. Li, T. Thorsen, Z. Xu, Z. P. Fang, J. Zhao, et al., Appl. Optics 48, 5088 (2009).
[21] R. Mercatelli, S. Soria, G. Molesini, F. Bianco, G. Righini, et al., Opt. Express 18, 20505 (2010).
[22] A. Miks, J. Novak and P. Novak, Appl. Optics 49, 3259 (2010).
[23] D. N. Fuller, A. L. Kellner and J. H. Price, Appl. Optics 50, 4967 (2011).
[24] M. C. Hutley and R. F. Stevens, J. Phys. E Sci. Instrum. 21, 1037 (1988).
[25] D. Mendlovic, Opt. Commun. 95, 26 (1993).
[26] H. J. Tiziani, R. Achi and R. N. Kramer, J. Mod. Optic 43, 155 (1996).
[27] S. L. Dobson, P.-C. Sun and Y. Fainman, Appl. Optics 36, 4744 (1997).
[28] S. Sinzinger, V. M. Arrizon and J. Jahns, Proc. SPIE 3002, 186 (1997).
[29] P. C. Lin, P.-C. Sun, L. Zhu and Y. Fainman, Appl. Optics 37, 6764 (1998).
[30] S. Cha, P. C. Lin, L. Zhu, P.-C. Sun and Y. Fainman, Appl. Optics 39, 2605 (2000).
[31] R. J. Garzón, J. Meneses, G. Tribillon, T. Gharbi and A. Plata, J. Opt. A Pure Appl. Opt. 6, 544 (2004).
[32] K. Körner and A. Ruprecht, Anordnung und Verfahren zur hochdynamischen, konfokalen Technik, Patent DE10321884A1 (2004).
[33] A. K. Ruprecht, C. Pruss, H. J. Tiziani, W. Osten, P. Lucke, et al., Proc. SPIE 5856, 128 (2005).
[34] J. Garzon, T. Gharbi and J. Meneses, J. Opt. A Pure Appl. Opt. 10, 104028 (2008).
[35] A. Ruprecht, Konfokale Sensorik zur Hochgeschwindigkeits – Topografiemessung technischer Objekte (Dissertation, ITO, University Stuttgart, 2008).
[36] J. Garzon, D. Duque, A. Alean, M. Toledo, J. Meneses and T. Gharbi. J. Phys.: Conf. Ser. 274, 012069 (2011).
[37] M. Hillenbrand, C. Wenzel, X. Ma, P. Feßer and S. Sinzinger, in '8th EOS Topical Meeting on Diffractive Optics', Ed. by J. Tervo and P. Urbach (EOS – Events & Services GmbH, Hannover, 2012).
[38] M. Born, E. Wolf and A. Bhatia, in 'Principles of Optics', 7th ed. (Cambridge University Press, Cambridge, 2005).
[39] S. Sinzinger and J. Jahns, in 'Microoptics', 2nd ed. (Wiley-VCH, Weinheim, 2003).
[40] A. G. Schott, in 'Optical Glass Catalogue' (Mainz, Germany, 2011).
[41] M. Gu, in 'Principles of Three-dimensional Imaging in Confocal Microscopes' (World Scientific, Singapore, 1996).
[42] H. Dammann, Optik 53, 409 (1979).
[43] B. H. Kleemann, M. Seesselberg and J. Ruoff, J. Eur. Opt. Soc. Rap. Publ. 3, 8015 (2008).
[44] K. P. Thompson, JOSA A 22, 1389 (2005).
[45] W. Richter and B. Mitschunas, F M-Feinwerktech. Mes. 100, 459 (1992).
[46] W. T. Welford, in 'Aberrations of Optical Systems', Amended repr. (Taylor & Francis, New York, 1991).

Matthias Hillenbrand holds an engineer's degree in mechanical engineering from Technische Universität Ilmenau. Currently, he works as a research assistant at Fachgebiet Technische Optik and is pursuing a doctoral degree in the field of optical engineering. His main research areas are the design of optical systems without symmetry and the development of systems for chromatic information coding.

Beate Mitschunas received her engineering and doctoral degrees from Technische Universität Ilmenau in 1978 and 1985, respectively. Since 1984, she has been employed as a research assistant at TU Ilmenau. Her fields of interest are the collinear and analytical modelling of imaging optical systems, holographic optical elements, and the development of non-conventional optical systems.

Christian Wenzel studied mechanical engineering with a focus on precision engineering and technical optics at Technische Universität Ilmenau. In 2011, he graduated with a Master of Science at TU Ilmenau. Currently, he works as a developer for optical systems at Hella KGaA in Lippstadt (Germany), a well-known supplier of the automotive industry.

Adrian Grewe studied mechanical engineering specialising in precision engineering and optics at Technische Universität Ilmenau. In 2010, he graduated with a diploma in engineering. Since then, he has worked for TU Ilmenau as a PhD student in the field of ultra-precision micro-milling of optical components and hyperspectral imaging.

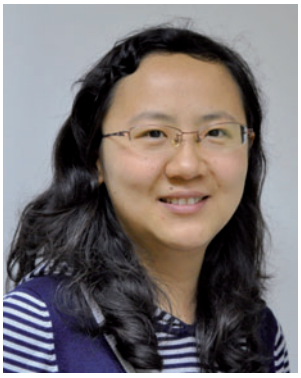

Xuan Ma received her Bachelor degree in 2003 from Beijing Institute of Technology. Then she studied mechanical engineering at Technische Universität Ilmenau in Germany and graduated in 2008 with an engineer's degree. Since 2009, she has worked on her PhD at Fachgebiet Technische Optik, TU Ilmenau.

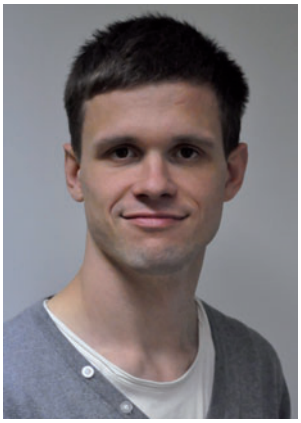

Patrick Feßer completed his apprenticeship as a microelectronics technician in 2011. Since then, he has worked as a technical employee at Technische Universität Ilmenau. His fields of activity include lithography on planar and non-planar substrates as well as the fabrication and characterisation of diffractive optical elements.

Mohamed Bichra studied Micro and Medical Technology with a particular focus on laser systems at the University of Applied Sciences Gelsenkirchen. In 2009, he graduated with an engineering degree from the same university. Between 2008 and 2012, he has worked as a development engineer at Limo Lissotschenko Mikrooptik GmbH in Dortmund and at Heinz Group in Elgersburg. Since 2012, he is a PhD student and research assistant with Prof. Sinzinger at Technische Universität Ilmenau.

Stefan Sinzinger received his Dipl.-Phys. and Dr. degrees from the Friedrich-Alexander Universität Erlangen-Nürnberg, Institute for Applied Optics (Prof. Dr. A.W. Lohmann) in 1989 and 1993, respectively. In 2002, he became Professor for Optical Engineering ('Technische Optik') at the Technische Universität Ilmenau. Among more than 160 publications in international journals and conferences, Stefan Sinzinger is co-author of the textbook 'Microoptics' and editor of the textbook 'Optical Information Processing' (author A.W. Lohmann). His current research focuses on the design, integration, fabrication, and application of (micro-) optical elements and hybrid optical (micro-) systems.